ELSEVIER

Nuclear Instruments and Methods in Physics Research A 417 (1998) 182–196

NUCLEAR INSTRUMENTS & METHODS IN PHYSICS RESEARCH Section A

Nuclear tensor polarization in a laser-driven polarized deuterium internal target

J.A. Fedchak[1], K. Bailey, W.J. Cummings*, H. Gao[2], R.J. Holt[3], C.E. Jones[4], R.S. Kowalczyk, T. O'Neill, M. Poelker[5]

Physics Division, Argonne National Laboratory, Argonne, IL 60439-4843, USA

Received 6 February 1998; received in revised form 22 April 1998

Abstract

We present the results of the first direct measurement of nuclear polarization in an optically pumped spin-exchange polarized deuterium target. Measurements of the nuclear tensor polarization p_{zz} are made in a storage cell as a function of flow of deuterium nuclei. For these measurements, the optical pumping was performed on atoms in magnetic fields of 600 and 3600 G. These measurements verify that the spin-exchange method is capable of producing polarized deuterium nuclei without the use of rf transitions. The electronic polarization, P_e, is also measured. The P_e and p_{zz} measurements at 600 G indicate that the system is in spin-temperature equilibrium, whereas the 3600 G measurements show signatures of non-equilibrium effects. P_e is also measured with the system operated as a source of polarized atoms, with no storage cell. These measurements are compared with previous measurements using a similar source.

PACS: 29.25Pj; 32.80Bx; 42.62-b

1. Introduction

There has been a continuing effort at Argonne National Laboratory to apply a spin-exchange optical pumping technique to polarize a gas of hydrogen or deuterium [1–3]. The aim of this effort is to produce a nuclear polarized internal target for use in scattering experiments at storage ring facilities such as the VEPP-3 electron storage ring at Novosibirsk, the IUCF cooler ring in Indiana, the MIT-Bates electron storage ring, the AmPS storage ring at NIKHEF in Amsterdam, and the HERA storage ring at DESY in Hamburg. To polarize the hydrogen or deuterium using the spin-exchange optical pumping method, potassium atoms are first polarized by optical pumping in a high magnetic field with polarized laser light. Electron polarization passes from K to H or D in spin-exchange collisions. The electron polarization is

* Corresponding author. Tel. +1 630 252 3431; fax: +1 630 252 3903; e-mail: cummings@anl.gov.

[1] Present address: Department of Physics, University of Wisconsin, Madison, WI 53706, USA.

[2] Present address: Department of Physics, Massachusetts Institute of Technology, Cambridge, MA, USA.

[3] Present address: Department of Physics, University of Illinois, Urbana, IL 61801, USA.

[4] Present address: Kellogg Lab 106-38, Caltech, Pasadena, CA 91125, USA.

[5] Present address: TJNAF, Newport News, VA 23606, USA.

0168-9002/98/$19.00
PII: S0168-9002(98)00738-4

subsequently transferred to the hydrogen or deuterium nuclei through D–D or H–H spin-exchange collisions. Polarized atoms flow from the optical pumping region into an open ended storage cell (typically an aluminum tube) which serves as a target for a scattering experiment.

The technique of spin-exchange optical pumping has been known for some time and is routinely used to produce polarized ^{3}He targets in nuclear physics experiments designed to study spin-dependent properties of nucleons and nuclei [4]. However, there are several technical challenges in producing a polarized H or D target which distinguish it from the polarized ^{3}He targets. Noble gas atoms interact very little with each other or with surfaces; i.e., the spin-relaxation time for polarized ^{3}He in a sealed glass cell containing Rb may be tens or hundreds of hours [5]. In contrast, the hyperfine interaction couples the hydrogen or deuterium nucleus to a single valence electron which, in turn, may strongly interact with a surface during a wall collision or with other atoms in gas-phase collisions. To reduce relaxation of electron spin, the internal surfaces of the laser-driven target are coated with organosilane compounds (known generically as "drifilm") which preserve electronic polarization in collisions with the walls. Even with this precaution, the timescale for spin-relaxation due to wall collisions is on the order of 10 ms in the laser-driven target. On the other hand, H–K and D–K spin-exchange rates are fairly fast and the atoms become polarized on a timescale of milliseconds. This allows one to operate the laser-driven target in a continuous flow mode where the H or D atoms need to spend only a few milliseconds in a spin-exchange region to become polarized. The presence of K in the system complicates this fairly straightforward polarization process because alkalis are known to destroy drifilm coatings, and the walls of the apparatus must be heated to prevent the alkali from condensing on the surfaces. In addition, H or D atoms may recombine on the surfaces to form molecules, thus resulting in a loss of atomic fraction. Therefore the coating must also preserve atomic fraction.

In spite of these technical challenges, the development of laser-driven optically pumped polarized H and D sources has been pursued because of its potential to deliver a greater flow of polarized gas than the traditionally used atomic beam source (ABS) [6]. For internal target experiments, this larger flow can lead to greater target thickness and shorter counting times. Consequently, a laser-driven source has been considered for the Hermes experiment [7]. The compact size of the laser-driven target makes it attractive in situations where spatial constraints restrict the use of an ABS, such as the experiments described in Ref. [8]. Additionally, the technology may eventually lead to the production of an external target of polarized tritium since, one could operate a spin-exchange target in a closed system where one would not have to deal with exhausting and disposing of radioactive tritium [9].

Now many of the technical challenges encountered in the development of a laser-driven polarized H and D source have been met sufficiently to produce a polarized deuterium and hydrogen target [10]. Here we will present the most recent polarization measurements made at Argonne, where the laser-driven D source is connected to a storage cell in an internal target configuration, and the nuclear tensor polarization in the storage cell is directly measured. These nuclear tensor polarization measurements represent the first systematic study of nuclear polarization made on the laser-driven target. Preliminary results verifying that deuterium can obtain nuclear polarization through spin-exchange collisions were first reported by Fedchak et al. [11]. Signatures of spin-temperature equilibrium, discussed below, were observed. Evidence that spin-temperature equilibrium is achievable in laser-driven H and D sources was first observed by Poelker et al. [2]. This was subsequently confirmed by Stenger et al. [12] for polarized H sources.

2. Spin-temperature equilibrium

Unlike the ABS, the laser-driven target does not depend upon the use of a Stern–Gerlach magnet to obtain polarized atoms or the use of rf transitions to transfer electron polarization to the nucleus. Instead, D atoms are polarized in K–D spin-exchange collisions and atomic angular momentum is redistributed among the deuterium magnetic

substates as a result of spin-exchange collisions between the D atoms. Hence spin-exchange collisions play a dual role in creating polarized nuclei in a laser-driven target. Again, this is a very different situation from that of an ABS where rf transition units are used to obtain nuclear polarization. In the ABS, one must minimize the spin-exchange collisions because collisions occurring before entering the rf transition unit tend to diminish the transition efficiency and collisions occurring after the atoms leave the rf transition unit tend to depolarize the beam. In the limit of many spin-exchange collisions, the relative population among the magnetic substates will reach a distribution unique to the total angular momentum pumped into the system. This limit is known as spin-temperature equilibrium and has an important impact on the design, operation, and understanding of a laser-driven hydrogen or deuterium target.

The physics of the laser-driven target can be understood by considering the nature of spin-exchange collisions in high magnetic fields. Here we define a high magnetic field as one larger than the critical field $B_c = \Delta W/(\mu_I + \mu_e)$, where ΔW is the hyperfine splitting at zero external B-field and μ_I and μ_e are the nuclear and electron magnetic moments. The critical field is 117 G for deuterium and 507 G for hydrogen. We will restrict the following discussion to D but make comments pertaining to H where appropriate. Walker and Anderson [13] have examined the consequences of spin-exchange in systems of H or D atoms. They derived rate equations that describe the population distribution of the six magnetic substates of D (see Fig. 1) in an external B-field. Spin exchange collisions between D atoms will redistribute the angular momentum amongst the various magnetic substates and drive the system towards an equilibrium population distribution consistent with the z-component of the total angular momentum $\langle F_z \rangle$. At steady state, the system can be characterized by a spin-temperature β^{-1}, so that the population of any particular substate is given by

$$\rho(m_F) = \frac{1}{N} e^{\beta m_F}. \tag{1}$$

Accordingly, at equilibrium, the z-component of the total angular momentum is related to the spin-temperature by

$$\langle F_z \rangle = \frac{3\sinh(\frac{3}{2}\beta) + 2\sinh(\frac{1}{2}\beta)}{2\cosh(\frac{3}{2}\beta) + 4\cosh(\frac{1}{2}\beta)}. \tag{2}$$

It is thus seen that β is characteristic of the net angular momentum pumped into the system. Eq. (1) can be used to calculate the electronic polarization P_e, the nuclear vector polarization p_z, and the nuclear tensor polarization p_{zz}, at equilibrium, shown in Fig. 2.

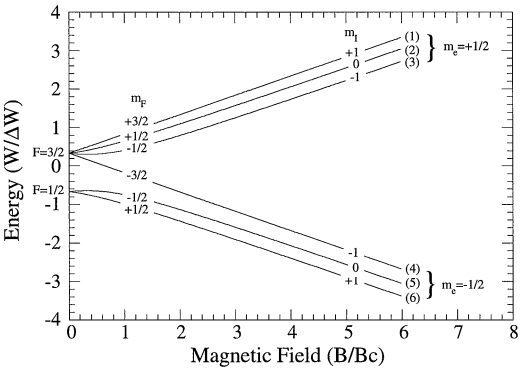

Fig. 1. The energy W of the deuterium hyperfine substates as a function of external B-field in units of the critical field, $B_c = 117$ G. $\Delta W = h \times 327.4$ MHz is the energy of the hyperfine splitting in zero external B-field.

Several important characteristics of spin-temperature equilibrium are revealed in Fig. 2. At equilibrium, one only needs to measure a single polarization, i.e. P_e, p_z, or p_{zz}, to determine the magnitude of the remaining two. The nuclear tensor polarization p_{zz} is always positive because the $m_I = 0$ substates tend to become depleted as the system approaches spin-temperature equilibrium. This is equally true for pumping with either σ_+ or σ_- light. The inequality $|p_z| \geq |P_e| \geq p_{zz}$ arises because the depletion of the $m_I = 0$ substates tend to raise $|p_z|$. For a system of H atoms, $p_z = P_e$ at equilibrium, which is a consequence of the fact that hydrogen has a spin $\frac{1}{2}$ nucleus so that the polarization is evenly divided between P_e and p_z at equilibrium. For both hydrogen isotopes, it is also important to note that once spin-temperature equilibrium is reached, the population distribution is independent of any external magnetic field [14]. Therefore, changing the

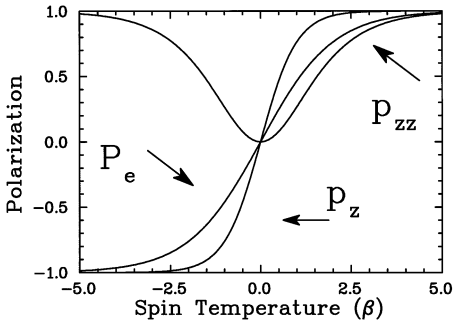

Fig. 2. The electronic polarization P_e, nuclear vector polarization p_z, and nuclear tensor polarization p_{zz} of deuterium as a function of β at spin-temperature equilibrium. β^{-1} is the spin-temperature and is characteristic of the total angular momentum pumped into the system.

external B-field will not change the electron or nuclear polarization.

The time required to reach equilibrium depends on the external magnetic field, the deuterium number density n_D, and the D–D spin-exchange cross section σ_{SE}. It is approximately given by

$$T_{ST} \approx \left(1 + \left(\frac{B}{B_c}\right)^2\right) \frac{1}{n_D \langle \sigma_{SE} v \rangle}, \tag{3}$$

where v is the thermal velocity. For this system, where the laser light only directly polarizes the atomic electrons, T_{ST} is the timescale for the nucleus to become polarized. For example, in the system used for the measurements described here, $T_{ST} \approx 0.6$ ms for a D flow of 2×10^{17} nuclei/s and $B = 600$ G, whereas $T_{ST} \approx 19.5$ ms for the same flow when the external field is increased to 3.6 kG. These values should be compared to the average dwell time for a D atom in the optical pumping cell $T_{dwell} = 5.7$ ms. An average D atom spends an additional 5.3 ms in the transport tube and storage cell, where no optical pumping takes place. It would seem that the lower the external field, the higher the polarization because once spin is transferred to the nuclei, the D atom can be repolarized in a spin-exchange collision with polarized K atoms. However, if the external field becomes too low, the K polarization will be limited by radiation trapping, the reabsorption of depolarizing fluorescent photons as the absorption profile of the σ_+, σ_-, and π transitions overlap at low B-fields [15]. Spin relaxation of alkalis on surfaces is also known to increase as the external B-field is lowered but should not limit polarization for B-fields above 500 G [16].

Stenger and Rith [17] have explicitly written the rate equations derived by Walker and Anderson in terms of rate constants relevant to the laser-driven target. There are a total of nine coupled rate equations, corresponding to the six magnetic substates of D and three states of K (two ground substates and one excited). They modeled the Argonne system without the storage cell and obtained good agreement with published laser-driven source data by adjusting parameters in the rate constants. The presence of the storage cell makes the task more difficult. In particular, the magnetic field gradient along the transport tube and storage cell is difficult to handle computationally, and many of the relevant rate constants are unknown. Spin relaxation due to collisions of polarized atoms with molecular deuterium is not included in this model, nor is the radiation trapping effect mentioned above. Additionally, in order to properly include optical pumping in the model, it will be necessary to include the K substates associated with nuclear spin since spin-exchange collisions strongly affect the optical pumping process by transferring spin between the electron and nucleus [18].

3. Experimental apparatus

3.1. Optical pumping cell and P_e polarimeter

In Fig. 3 we show details of the Pyrex glassware which comprises the dissociator, optical pumping cell, and most of the transport tube. A schematic of the entire laser-driven target system is shown in Fig. 4, including the optical pumping system, Pyrex glassware, probe laser system, storage cell, nuclear (p_{zz}) polarimeter, and atomic (P_e) polarimeter. Deuterium flows into the dissociator where a 49 MHz radio-frequency discharge dissociates the molecular deuterium into atoms. Deuterium atoms and molecules flow from the dissociator into a cylindrical optical pumping cell which lies between two pole faces of an electromagnet. The optical

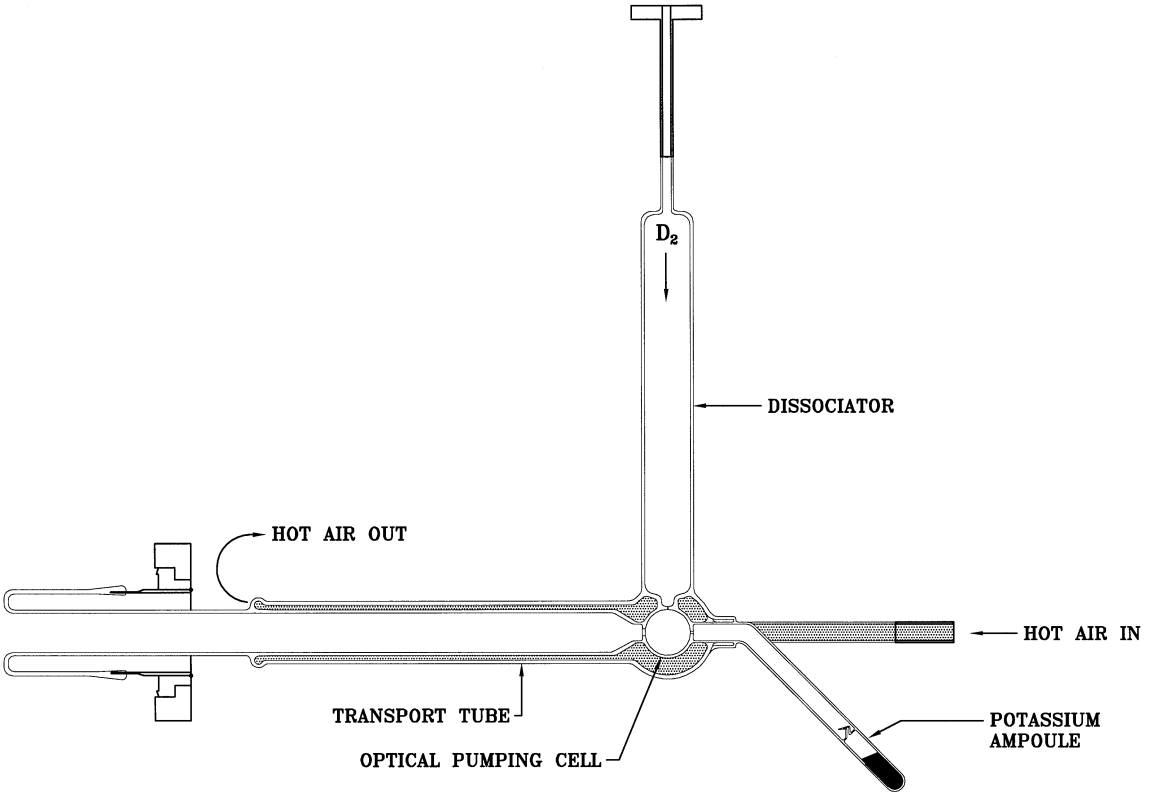

Fig. 3. Cross-sectional diagram of the Pyrex glassware used in the laser-driven source.

pumping cell has a diameter of 2.2 cm and a length of 4.6 cm. The direction of the *B*-field points along the length of the optical pumping cell, and the magnitude is constant in the pumping cell and is adjustable from 0 to 4 kG. Potassium enters the cell through a 0.9 mm aperture connected to an ampoule containing a K reservoir heated to 160 – 180°C. A probe laser technique, discussed in Section 2.3, is used to measure the K density in the optical pumping cell.

The $4^2S_{1/2} - 4^2P_{1/2}(D_1)$ resonance of K is optically pumped by ~ 2 W of circularly polarized light incident on the optical pumping cell along the axis of the *B*-field. A Ti:sapphire ring laser pumped by a 18 W Ar-ion laser is used as the light source. The laser light is broadened to about 1 GHz by an electro-optical modulator to match the Doppler width of the σ_+ and σ_- transitions. Further details of the laser system can be found in Refs. [2,3].

Atoms experience about 700 wall bounces in the pumping cell and enter the transport tube through a 3.1 mm aperture. The pumping cell and Pyrex transport tube are heated to between 200°C and 250°C by flowing hot air through a surrounding Pyrex jacket. The magnetic field decreases continuously along the length of the transport tube, falling by a factor of one-half at a distance of 9 cm from the pumping cell. The Pyrex transport tube extends to a length of 30 cm and has a diameter of 19 mm.

The system can be operated in two configurations. In the first configuration, the system is operated as a source of polarized atoms so that atoms exiting the Pyrex transport tube are subsequently detected in the P_e polarimeter. In the second configuration, the system is operated as a polarized target. In this configuration the Pyrex transport tube is extended by an aluminum tube 6 cm in length. The diameter of the aluminum transport

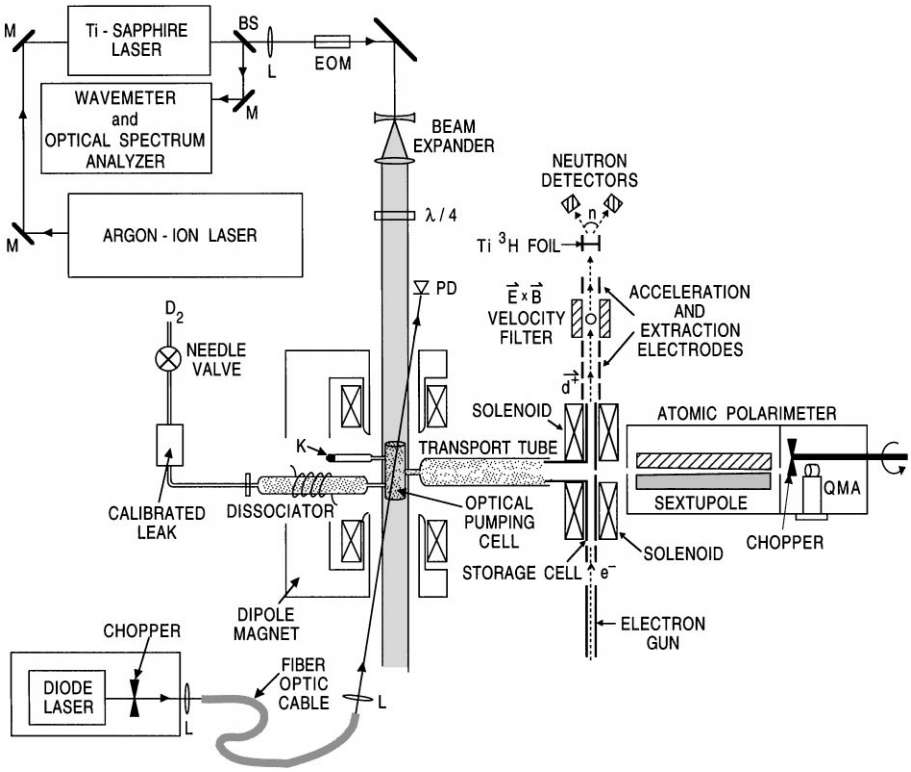

Fig. 4. Schematic diagram of the entire laser-driven target. (BS) beam splitting optic, (L) lens, (M) mirror, (PD) photo-diode, (QMA) quadrupole mass analyzer.

tube is 1.6 cm. This is joined to the glassware with a viton O-ring. Atoms exiting the extended transport tube flow into an open ended aluminum storage cell, discussed further in Section 3.2. A 5 mm hole in the center of the storage cell allows the P_e polarimeter to sample atoms leaving the transport tube.

The P_e polarimeter is located downstream of the transport tube and has an acceptance such that the polarimeter samples atoms whose last wall bounce occurs between the exit aperture of the optical pumping cell and the cylindrical wall of the transport tube. Therefore, on average the atoms sampled by the P_e polarimeter have made many wall collisions in the transport tube. A sextupole magnet focuses atoms with electron spin up and defocuses those with spin down. Focused atoms pass through a chopper wheel and are detected by a quadrupole mass analyzer (QMA). A removable shutter placed before the sextupole allows one to measure the background signal in the QMA. Atomic polarization can be measured by blocking and unblocking the pump laser beam. The atomic or electronic polarization is determined by

$$P_e = \frac{n_\uparrow - n_\downarrow}{n_\uparrow + n_\downarrow} = \frac{n_{\text{unblocked}}}{n_{\text{blocked}}} - 1, \tag{4}$$

where $n_{\uparrow(\downarrow)}$ denotes deuterium atomic states with electron spin up (down) and $n_{\text{(un)blocked}}$ is the signal measured with the QMA with the laser beam (un)blocked.

The P_e polarimeter is also used to measure the atomic fraction, f_a, defined as the total number of deuterium nuclei in atoms over the total number of deuterium nuclei in either atoms or molecules. This is determined with the QMA by measuring the mass 4 (amu) signal with the dissociator rf power on

and off:

$$f_a = 1 - \frac{n_{on}}{n_{off}}. \quad (5)$$

With the rf power off, the mass 4 signal n_{off} is entirely due to D_2, but when the dissociator rf power is turned on the mass 4 signal, n_{on}, measures the molecular flow from D_2 molecules that are not dissociated before entering the optical pumping cell and that form due to recombination on surfaces between leaving the dissociator and being detected in the QMA. For both f_a and P_e, the error in the measurements are dominated by systematic uncertainties and is less than 2% of the measured values.

In order to reduce the recombination on surfaces as well as preserve D and K polarization, the optical pumping cell, transport tube and storage cell are coated with organosilane compounds known in the literature as drifilm. In particular, the Pyrex surfaces are coated using SC-77[6] plus a trichloromethoxysilane "afterwash" described in Fedchak et al. [19]. The aluminum storage cell and short connecting tube are coated with a mixture of dimethyldichlorosilane and methyltrichlorosilane also discussed in Ref. [19].

3.2. p_{zz} polarimeter

In addition to P_e, we can also measure the nuclear tensor polarization p_{zz}, defined by

$$p_{zz} = \frac{n_+ + n_- - 2n_0}{n_+ + n_- + n_0}, \quad (6)$$

where n_+, n_-, and n_0 represent the population densities of nuclear spin substates $m_I = +1, -1$, and 0, respectively. The polarimeter is based upon the technique developed by Price and Haeberli [20]. To determine p_{zz} the polarimeter employs the low energy $D + {}^3H \rightarrow n + {}^4He$ reaction in which the angular distribution of the outgoing neutrons is anisotropic if the incident deuterium ions are tensor polarized. At low energy the ${}^3H(D,n){}^4He$ reaction can proceed through both $J^\pi = 3/2^+$ and $J^\pi = 1/2^+$ resonances in ${}^5He$. The unpolarized cross section has a broad resonance peak centered at a deuteron energy of 110 keV, corresponding to the $J^\pi = 3/2^+$ channel, which dominates the cross section at low energy. The expression for the differential cross section for a tensor-polarized incident deuteron beam is

$$\left(\frac{d\sigma}{d\Omega}\right) = \left(\frac{d\sigma}{d\Omega}\right)_0 \left(1 - \frac{f_d}{4} p_{zz} (3\cos^2\theta - 1)\right). \quad (7)$$

$(d\sigma/d\Omega)_0$ is the unpolarized cross section, which is isotropic in the center-of-mass frame, θ is the angle between the direction of the outgoing neutron and the spin of the deuteron in the center-of-mass system, p_{zz} is the tensor polarization of the deuteron, and the dilution factor f_d accounts for the small admixture of the $J^\pi = 1/2^+$ reaction channel which has no tensor analyzing power. The dilution factor has been measured and found to be near unity ($f_d \approx 0.96$) for ion energies in the range used for the polarimeter [21]. The neutron anisotropy R, defined as

$$R = \frac{(d\sigma/d\Omega)(0^\circ)}{(d\sigma/d\Omega)(90^\circ)} = \frac{1 - (f_d/2)p_{zz}}{1 + (f_d/4)p_{zz}} \quad (8)$$

is determined from the ratio of neutron intensities detected in scintillators placed at 0° and 90°. The ratio of the measured R values for polarized and unpolarized ions is used to determine the tensor polarization of the deuterons in the storage cell. Differences in the detector efficiencies and angular acceptance largely cancel in the background subtracted ratio. The finite angular acceptance of the detectors leads to a slightly different analyzing power than shown in Eq. (7). The size of this effect is included in the systematic error discussion at the end of this section.

The p_{zz} polarimeter is shown in the schematic drawing of the apparatus, Fig. 4. With the apparatus configured as an internal target, particles exit the optical pumping cell and flow through a transport tube into the storage cell, a cylindrical aluminum tube of 48 cm length and 23 mm diameter. Both the storage cell and Al section of the transport tube are heated to over 200°C. The storage cell and transport tube are coated with drifilm to reduce recombination and depolarization on the surface. A small hole in the storage cell opposite the connection to the transport tube allows the P_e polarimeter

[6] SC-77 is a mixture of dimethyldichlorosilane and methyltrichlorosilane available from Silar Industries.

to sample a small fraction of the atoms entering the storage cell. Because of its solid angle acceptance, the P_e polarimeter samples atoms scattered from the walls of the transport tube, rather than the walls of the storage cell. In contrast to the atomic polarimeter, the p_{zz} polarimeter samples atoms from throughout the storage cell.

A solenoidal coil surrounding the storage cell creates the magnetic holding field that serves both to decouple the electronic and nuclear spins and as a guide field for the ions to prevent them from hitting the cell walls. The longitudinal holding field is 300 G over most of the length of the storage cell; the value at the center of the cell where the atoms enter from the transport tube drops to 140 G.

A 2 keV electron beam directed along the length of the storage cell ionizes the deuterium atoms to produce D^+. Ions are extracted from the storage cell and accelerated towards a tritiated foil target mounted inside an electrostatic lens maintained at a potential of 44 kV. A Wein filter ($\boldsymbol{E} \times \boldsymbol{B}$) located between the storage cell and tritiated foil acts as a velocity selector to separate deuterium atoms and molecules. Fig. 5 shows the measured resolution of the filter, which could readily resolve D^+ and D_2^+. The deuteron spin direction, which is parallel to the solenoidal holding field in the storage cell, precesses by 45° in the B-field of the Wein filter. Neutrons resulting from the fusion reaction $^3H(D,n)^4He$ are detected in two NE110 scintillators placed parallel and perpendicular to the spin direction, thus maximizing the neutron anisotropy in the two detectors. Each scintillator is coupled to two phototubes and a valid neutron count is defined by a coincidence between these two phototubes.

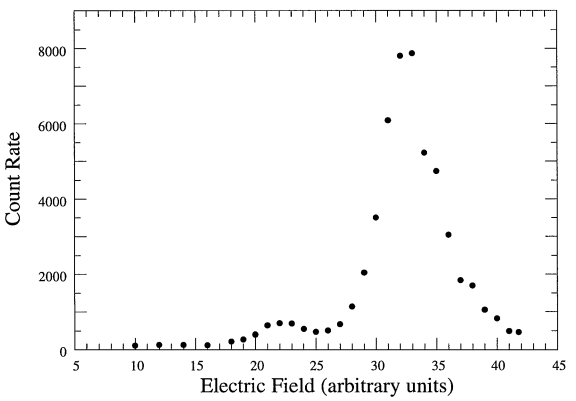

Fig. 5. The total neutron count rate detected in the two scintillators as a function of the electric field between the two plates of the $\boldsymbol{E} \times \boldsymbol{B}$ velocity filter. The B-field of the filter is held constant for these measurements.

Tests of the polarimeter with unpolarized deuterium show that the measurements are reproducible to better than $\Delta R/R = 0.004$. Corrections for the variation of p_{zz} due to the angular acceptance contribute an uncertainty of $\Delta p_{zz}/p_{zz} < 0.005$. The overall systematic error is dominated by the uncertainty in the spin rotation angle in the Wien filter, which gives a contribution of $\Delta p_{zz}/p_{zz} < 0.065$. For the p_{zz} data presented in this paper, all measurements were repeated many times and checked to make sure that they were statisically consistent. The results presented are the average of these measurements with its statistical error.

3.3. K density measurements

Potassium density and polarization are measured by observing the attenuation of a low power beam from a single-mode diode laser transmitted through the optical pumping cell as this probe laser is tuned across the $4^2S_{1/2} - 4^2P_{1/2}$ transition of potassium. The technique is similar to that described in Poelker et al. [2,3]. A simplified diagram of the probe laser setup is included in Fig. 4. Approximately 5 μW of light from the diode is focused into a multi-mode fiber optic. Other than a focusing lens attached to the end of the fiber optic, no focusing or polarizing optics are used on the probe beam after exiting the optical fiber. The probe beam is directed through the optical pumping cell in a direction opposite to the pumping beam from the Ti:sapphire laser and the intensity of the transmitted light is monitored with a photodiode. For the polarization measurements, the probe beam is chopped before being focused into the fiber so that the transmitted light can be detected with a lockin amplifier to reduce the background noise from scattered light from the primary polarizing beam. The frequency of the diode laser is continually scanned across the $4^2S_{1/2} - 4^2P_{1/2}$ transition of potassium by adjusting the diode current. The laser is swept over a range of about 30 GHz, far wider than the 1 GHz linewidth of the absorption profile

of the D_1 transition. Two secondary beams are split off from the primary probe beam before it is focused into the fiber optic. One secondary beam is directed into a reference cell containing potassium heated to 75°C, which is used to monitor the resonant frequency of the D_1 transition in zero B-field. The other secondary beam is focused into a Fabry–Perot spectrum analyzer which has a free spectral range of 7.5 GHz and is used to check the probe beam for mode-hops and to calibrate the frequency scale of the absorption profile scans.

The intensity of the probe laser light transmitted through the cell, $I(v)$, is related to the K density n_K by

$$I(v) = I_o e^{-n_K l \sigma(v)}, \tag{9}$$

where v is the laser frequency, I_o is the intensity of the probe beam incident upon the optical pumping cell, l is the length of the cell, and $\sigma(v)$ is the absorption cross section. The absorption cross section can be written in terms of the known oscillator strength f as $\sigma(v) = \pi c r_e f L(v - v_o)$, where v_o is the resonant frequency of the transition, r_e is the classical electron radius, and $L(v - v_o)$ is the normalized lineshape. The lineshape of the absorption cross section is dominated by Doppler broadening which is described by a Gaussian profile. The natural linewidth, collisional and pressure broadening contribute a Lorentzian component to the lineshape, so the measured lineshape is theoretically more accurately described by a Voigt profile and we use this lineshape in our fits to the absorption data.

We determined n_K from the absorption scans by fitting the right-hand side of Eq. (9) to the measured $I(v)$, fixing the Gaussian width to the Doppler width and allowing the Lorentzian width, the incident intensity, the position of the resonant frequency and the density to vary. In practice, the diode laser intensity varied linearly with frequency, so for the purposes of the fit we modeled $I_o(v)$ as a straight line. Under typical operating conditions, the potassium density was sufficiently high to completely absorb the probe beam for frequencies near v_o. The fits we obtained using a small Lorentzian contribution, ~ 5–10% the width of the Gaussian, were significantly better in the wings of the absorption profile than we could obtain using a Gaussian profile alone. The Lorentzian width was consistent across all data sets taken over a period of approximately half a year.

The potassium density in the optical pumping cell is controlled by adjusting the temperature of the K reservoir using a heater wrapped around the potassium ampoule. Fig. 6 shows n_K measured in the optical pumping cell as a function of K reservoir temperature T_K. Experimental systematic uncertainties dominate the error in the measurements and are reflected in the plotted error bars. Several measurements were made at each reservoir temperature over a time span of several months, and the values obtained for the K density were repeatable to within $\leq 10\%$. The two measurements plotted at $T_K = 170^\circ$ show "worse case" variations obtained for different glassware.

Measuring the potassium polarization P_K is somewhat more difficult because of a sizable background signal from the pumping beam and fluorescent light. The signal-to-noise ratio (SNR) is improved by chopping the probe laser beam and using a lockin amplifier to detect the signal from the photodiode. Since P_K must be determined with the magnetic field on, two minima in the absorption profile are observed, corresponding to the σ_+ (spin up) and σ_- (spin down) transitions. To determine P_K we use a fit similar to that used for n_K, allowing the K density in each absorption minima to vary. The polarization is determined from the

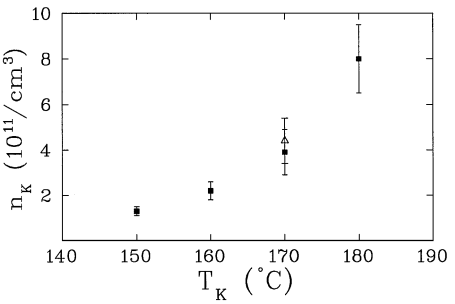

Fig. 6. The potassium density n_K in the optical pumping cell measured using a laser probe technique and expressed as a function of K reservoir temperature T_K. The temperature of the Pyrex optical pumping cell is maintained between 200°C and 250°C.

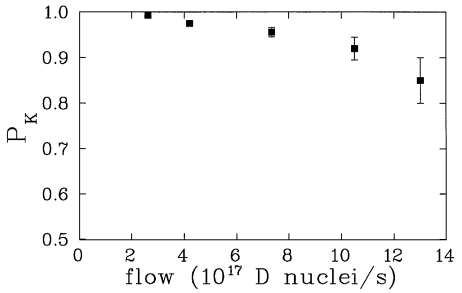

Fig. 7. The potassium polarization P_K in the optical pumping cell as a function of the flow of deuterium nuclei. The data was taken at $T_K = 180^\circ$ and a magnetic holding field of $B = 1.1$ kG.

densities as

$$P_K = \frac{n_\uparrow - n_\downarrow}{n_\uparrow + n_\downarrow}, \tag{10}$$

where $n_\uparrow$ and $n_\downarrow$ are the potassium population densities in the spin up and spin down states, in direct analogy to Eq. (4).

Fig. 7 shows P_K measured in the optical pumping cell as a function of deuterium flow for a K reservoir temperature of 180° and a magnetic field of 1.1 kG in the optical pumping cell. The plotted error bars are dominated by systematic uncertainties in the extraction of the densities in each magnetic substate. The polarization is observed to decrease at the highest deuterium flow, although the poor SNR limited our ability to quantify the decrease in K polarization.

4. Experimental results

In Section 4.1 we present P_e measurements made with the system operated as a source consisting only of the Pyrex glassware without a storage cell, while in Section 4.2 we present measurements with the system operated as a target with the aluminum storage cell and short aluminum connecting transport tube, discussed above. The atomic polarimeter samples atoms from the same location in the transport tube in both the source and target configurations. However, with the storage cell in place, the deuterium density is higher in the transport tube because of the decreased conductance. Therefore, the atoms sampled by the P_e polarimeter experience more spin-exchange collisions in a region where the B-field is of lower magnitude than in the optical pumping cell.

The nuclear tensor polarization p_{zz} can be measured in the storage cell. Atoms sampled by the p_{zz} polarimeter have experienced more wall bounces and gas-phase collisions than those sampled by the P_e polarimeter. Both p_{zz} and P_e were measured concurrently with the storage cell in place, and these results are reported in Section 4.2.

4.1. Polarized source configuration

Fig. 8 shows both the electron polarization P_e and the atomic fraction f_a as a function of flow of deuterium nuclei for $n_K = 8.0 \pm 1.5 \times 10^{11}\,\mathrm{cm}^{-3}$ and $B = 850$ G in the optical pumping cell. Both measurements were made simultaneously by switching the QMA tuning between mass 2 and 4. These measurements represent typical values obtained in the source configuration. At the highest flow where measurements where made $f_a = 0.41$, whereas for flows less than 10^{18} nuclei/s the atomic fraction varied from $f_a = 0.52$ to $f_a = 0.56$. For these lower flows, there is not a strong dependence of f_a on deuterium density. On the other hand, P_e has a strong dependence on flow for deuterium flows less than 7.0×10^{17} nuclei/s. Because T_{ST} depends on n_D, the electron polarization P_e rapidly decreases as the system approaches spin-temperature equilibrium and electron polarization is transferred

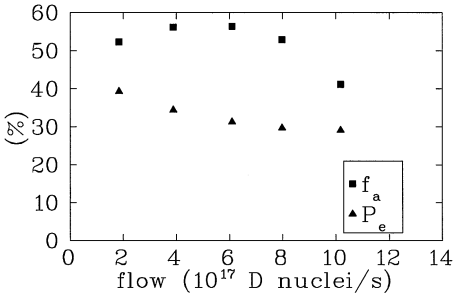

Fig. 8. The electronic polarization P_e and atomic fraction f_a measured as a function of flow of deuterium nuclei with the apparatus in the source configuration. The data was taken at $T_K = 180^\circ$ and a magnetic holding field of $B = 850$ G.

to the nucleus. The change in the slope of P_e for flows greater than 7.0×10^{17} nuclei/s is indicative that the system is in equilibrium at the higher D densities.

Poelker et al. [3] measured P_e versus flow in a source configuration similar to the present system. The present P_e measurements are 25–30% lower than the previous measurements made at $B = 1.2$ kG and $n_K = 4 \times 10^{11}$ cm^{-3}. There are several differences between these previous measurements and the present measurements which contribute to the smaller P_e values presented here. According to Eq. (3), T_{ST} is nearly twice as high at $B = 1.2$ kG than it is at $B = 850$ G. Therefore, in the present case, more angular momentum is stored in the nucleus as compared to the previous measurements, hence the measurements of Poelker et al. have higher P_e but should have correspondently lower nuclear polarization. Additionally, spin relaxation on surfaces has been observed to greatly increase as the external magnetic field is lowered [16], which may be a relevant effect in the transport tube where the field near the end of the tube falls by more than 10% of the field in the optical pumping cell. Therefore, spin relaxation in the transport tube is expected to be greater in the present experimental conditions. Presently, the Pyrex transport tube has a length of 30 cm compared to a length of 25 cm in the previous measurements. The longer of the two transport tubes has a conductance which is 15% smaller than the shorter tube. This reduced conductance results in a n_D which is larger in a region where the magnetic field is smaller than in the optical pumping cell, again increasing the wall relaxation. Finally, Poelker et al. report that 90% of the atoms sampled by the polarimeter have interacted with the walls in the transport tube, whereas in the present case, all the atoms sampled by the polarimeter interact with the walls of the transport tube. This means that in the present case, atoms have, on the average, experienced more depolarizing wall bounces and more spin-exchange collisions. In summary, atoms which enter the P_e polarimeter in the present system store a greater percentage of angular momentum in the nucleus and have experienced more wall collisions as compared to those in the system used by Poelker et al.

The dependence of P_e on K density in the pumping cell is illustrated in the measurements presented in Fig. 9. These measurements where made with a flow of 6.0×10^{17} nuclei/s and $B = 1.0$ kG. Although P_e is clearly increasing with the K reservoir temperature, T_K was not increased further to protect the drifilm coating from destruction [19]. This emphasizes the importance of wall coatings in the laser-driven target. Limitations of the coating technology are probably the greatest limiting factor on the obtainable polarization in the laser-driven target.

4.2. Internal target configuration

With the storage cell in place, both the electron polarization P_e and nuclear tensor polarization p_{zz} can be measured as a function of flow. Fig. 10 shows P_e and p_{zz} measurements at $B = 600$ G in the optical pumping cell. The error bars represent statistical and systematic uncertainties. The relative independence of P_e on flow is indicative that the system is in equilibrium over the entire range of flows investigated. Once n_D is great enough to achieve spin-temperature equilibrium, the dominant mechanism for losing polarization is the K–D collisions rate which is proportional to n_D (note that we distinguish this rate from the D–K collision rate which is proportional to n_K and does not depend on flow). Therefore, the decrease in P_e is reflected in the alkali polarization (see Fig. 7). This does not mean that P_K is a sensitive indication of

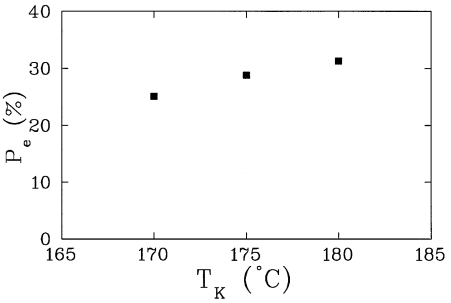

Fig. 9. The electronic polarization P_e versus potassium temperature T_K. T_K is a reproducible indicator of the potassium density in the optical pumping cell. All measurements are made at a deuterium flow of 6.0×10^{17} nuclei/s.

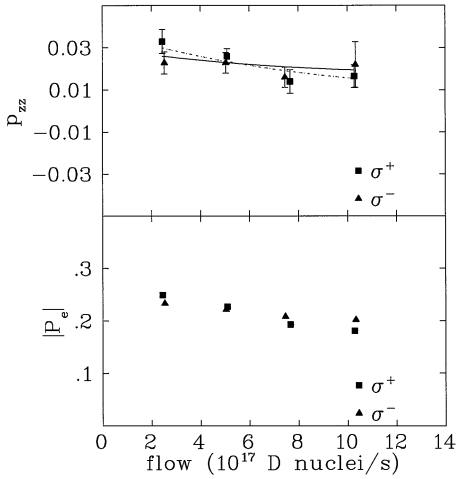

Fig. 10. The electronic polarization P_e and nuclear tensor polarization p_{zz} as a function of flow of deuterium nuclei for $T_K = 180^\circ$ and $B = 600$ G. The lines show the predictions for p_{zz} from the electron polarization measurements assuming spin temperature equilibrium and wall depolarization (see text). The solid line shows the expected p_{zz} from the corresponding P_e measurements with σ_- laser light. The dotted line is the prediction for the p_{zz} measurements with σ_+ light.

P_e, as a small change in P_K could result in large changes in P_e. Additionally, we have neglected other depolarization mechanisms which depend on D_2 density and hence flow, such as spin relaxation due to D–D_2 collisions and the loss of P_K due to K–D_2 collisions. To the authors knowledge, these spin relaxation rates have never been determined.

The helicity of the circularly polarized laser light was reversed to check for systematic effects. Other than the expected sign change, no dependence of $|P_e|$ on laser light helicity can be seen within the error of the measurements.

The measured p_{zz} is less than 0.035 for all the flows investigated. Presuming spin-temperature equilibrium, Fig. 2 can be used to determine the electron polarization expected from the p_{zz} measurements. On the average, the electron polarization inferred from spin-temperature, P_e^{ST}, is about 40% less than the P_e measurements presented in Fig. 10. Once the electron polarization is reduced by this amount, the p_{zz} expected shown by the solid and dotted lines in Fig. 10 are in good agreement with the measurements. This result is not surprising since the electron polarimeter samples atom from the transport tube, whereas the nuclear polarimeter samples along the length of the storage cell. Using Monte Carlo techniques, we estimate that the average D atom experiences about 1530 wall bounces between exiting the optical pumping cell and exiting the end of the storage cell, but experiences only 880 wall bounces before entering the electron polarimeter. Therefore, with $N = 650$, we can use the formula

$$P = P_0 e^{-N/N_{relax}} \tag{11}$$

to estimate the probability of relaxing per wall bounce, N_{relax}^{-1}. Letting $P \to P_e^{ST}$ and $P_0 \to P_e$, we calculate $\langle N_{relax} \rangle = 1370$ wall bounces. It must be noted that the electron gun of the nuclear polarimeter ionizes along the length of the storage cell, therefore 1530 wall bounces represents an upper limit to the number of wall bounces the average atoms has before detection in the nuclear polarimeter. $\langle N_{relax} \rangle$ could also be anomalously low due to poor coupling of the Pyrex transport tube to the aluminum tube, so that some of the atoms may interact with the viton O-ring which couples the two tubes, or enter the O-ring groove. Therefore in general $\langle N_{relax} \rangle$ does not reflect the effect of wall conditions alone.

For the measurements presented in Fig. 11, the field in the optical pumping cell was increased to 3.6 kG. As seen in the figure, the electron polarization decreases rapidly with flow; therefore, we conclude the system is not in spin-temperature equilibrium for the lower flows investigated. At the highest flow where data was taken, we calculate $T_{ST} = 3.9$ ms, recalling that $T_{dwell} = 5.7$ ms in the optical pumping cell. Therefore we expect that the system is close to being in equilibrium at the highest flow. The measured P_e at high flow is about one-half of that measured at the lowest flow where the system is relatively far from equilibrium. One would expect about a factor of two drop in P_e due to a loss of the electronic polarization to nuclear polarization. This is seen in the data. At the highest flow where data was taken, P_e is about 0.16 which, from spin-temperature equilibrium, implies $p_{zz} = 0.0034$. Taking into account a 40% reduction in polarization due to spin-relaxation, this is consistent with the measured p_{zz}.

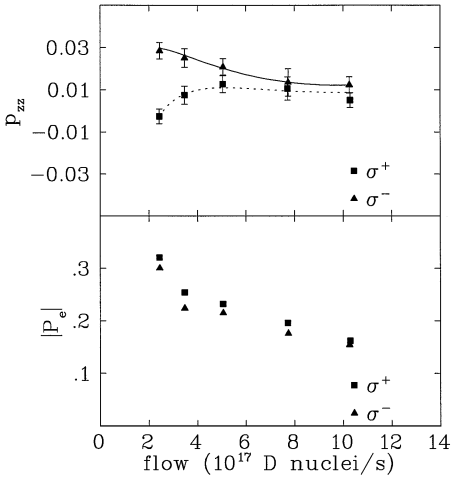

Fig. 11. The electronic polarization P_e and nuclear tensor polarization p_{zz} as a function of flow of deuterium nuclei for $T_K = 180^\circ$ and $B = 3.6$ kG. The lines correspond to a fit with a model in which only a fraction of the deuterium population has reached spin temperature equilibrium (see text). The dotted line is the fit result for the p_{zz} measurements with σ_+ laser light. The solid line shows the expected p_{zz} from the corresponding P_e measurements with σ_- laser light.

The behavior of p_{zz} is most notable. There is clearly a difference in the behavior of p_{zz} upon reversal of the helicity of the laser which is not due to systematic error. This behavior can be understood by assuming that the system is not in equilibrium and that the nuclear polarimeter may be sampling atoms from a region of low magnetic field. For example, the magnetic field in the storage cell falls to 140 G in the center of the cell near the entrance aperture of the transport tube. Additionally, it is possible that atoms are selectively ionized near the edge of the tube, where the magnetic field decreases to less than 200 G. Ion optics simulations indicate that this may indeed be the case. For a sample of D atoms not in spin-temperature equilibrium, i.e. those atoms not experiencing enough spin-exchange collisions to achieve the equilibrium population distribution, hyperfine coupling will mix magnetic substates in the $\langle |m_I m_e \rangle$ basis if the external field is lowered to near the critical field, B_c. As an extreme case, consider a system of D atoms which do not interact with each other but possess an electron polarization and no nuclear polarization at high field. For this case, we calculate p_{zz} as the field is lowered. In Fig. 12 we show results of this calculation for the conditions that $|P_e| = 1.0$ and $|P_e| = 0.19$ in the high field. From the figure, it is clear that, in this non-equilibrium situation, positive P_e at high-field yields negative p_{zz} at low field and vice versa.

We are now in a position to model the 3.6 kG tensor polarization data we obtained with the laser driven target. We assume that the system of D atoms can be separated into two groups: those which follow the spin-temperature equilibrium distribution of Fig. 2 and those which are in non-equilibrium and are described by the calculations of Fig. 12. The fraction of atoms in non-equilibrium is related to the flow of deuterium nuclei F_D by $f_{NE} = k/F_D$, where k is a constant. This follows from the observation that $f_{NE} \sim T_{ST}/T_{dwell}$. p_{zz} can then be written as the sum of equilibrium contributions, p_{zz}^{ST}, and non-equilibrium contributions, p_{zz}^{NE}:

$$p_{zz} = \left(1 - \frac{k}{F_D}\right) p_{zz}^{ST} + \left(\frac{k}{F_D}\right) p_{zz}^{NE}. \tag{12}$$

Both p_{zz}^{ST} and p_{zz}^{NE} are obtained from the measured electron polarization P_e. The measured P_e must first be reduced by a factor of 0.6, derived from the low field data and discussed above, to represent the electron polarization of the atoms sampled by the nuclear polarimeter. This reduced value of P_e is

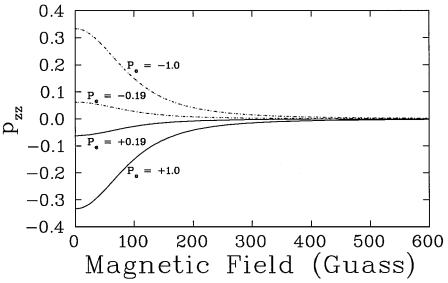

Fig. 12. The calculated nuclear tensor polarization p_{zz} for a system of deuterium atoms plotted as a function of magnetic field for the conditions that $P_e = \pm 1.0$ and $p_z = p_{zz} = 0$ at high field and $P_e = \pm 0.19$ and $p_z = p_{zz} = 0$ at high field. The system is not in spin-temperature equilibrium and no interactions between the atoms are assumed. Note that, in these conditions, it is not possible to obtain positive p_{zz} for optical pumping with σ_+ light.

used to infer p_{zz}^{ST} from Fig. 2. Similarly, the reduced P_e is used to calculate the non-equilibrium contribution p_{zz}^{NE}. However, p_{zz}^{NE} is also a function of the magnetic field at which the nuclear polarimeter samples, B_s. For this value, B_s is arbitrarily chosen to be 100 G. Modeling the p_{zz} data is then simply a matter of varying k to fit the data.

The dotted and solid lines in Fig. 11 represents results for $k = 1.6$, with F_D in units of $10^{17}\,s^{-1}$. The model is in excellent agreement with the data. According to the k value, 34% of the atoms follow the equilibrium distribution at the lowest flow investigated, whereas 85% follow the distribution at the highest flow shown. This is in accord with our estimate of T_{ST}, which indicates that the system should be close to spin-temperature equilibrium at the highest flow. While $B_s = 100$ G is slightly lower than expected, it is not bothersome considering the simplicity and crudeness of the model. More importantly, the model, while crude, accurately describes the data and provides a basis for understanding the physics involved in the curious "splitting" observed in the high field p_{zz} measurements.

It must be emphasized that this splitting does not occur for the $B = 600$ G measurements because the population distribution, and hence the polarization, does not depend on magnetic field once the system has reached spin-temperature equilibrium. This provides further evidence that the system is in equilibrium for the case of $B = 600$ G. Comparing the p_{zz} measurements made at 3.6 kG to those made at 600 G, non-equilibrium conditions have effectively raised the σ_- measurements and lowered the σ_+ from what one would normally expect for a system in spin-temperature equilibrium. There is no splitting effect in the P_e measurements because the atoms pass into the high field (> 3.6 kG) of the sextupole magnet which effectively decouples the electron spin from the nuclear spin. Spin up atoms in the high field of the sextupole are focused into the QMA, which is insensitive to the spin state.

The P_e measurements at high field exhibit a small dependence upon the pumping light helicity, a consequence of the frequency dependence of the laser output power. Unlike the high field p_{zz} measurements, the P_e measurements made with σ_- light are lower than those made with σ_+ light. As this is in contrast to the p_{zz} measurements, the helicity dependence of P_e cannot account for that observed in the p_{zz} data. A strong helicity dependence is not observed in the low field P_e measurements because the σ_- and σ_+ transitions are very close in frequency for atoms at a B-field of 600 G.

5. Conclusions

Nuclear tensor polarization and electron polarization have been measured in a laser-driven polarized D target. For P_e and p_{zz} measurements made with $B = 600$ G in the optical pumping cell, the combination of the relative independence of $|P_e|$ on flow and p_{zz} on the laser light helicity is indicative that spin-temperature equilibrium is achieved in the target. By increasing the magnetic field to 3600 G, we can see non-equilibrium effects in the polarization measurements, such as a rapid decrease in P_e with D flow, as well as a strong dependence of p_{zz} on the pumping light helicity. The latter effect can be explained by considering the B-field dependence of the magnetic substate population distribution. There is no B-field dependence if the atoms are in spin-temperature equilibrium. We have successfully modeled the high field p_{zz} measurements by considering that the system of D atoms consists partly of atoms in spin-temperature equilibrium and partly of atoms in non-equilibrium. Atoms following the equilibrium distribution possess polarizations independent of magnetic field, while those atoms not in equilibrium display field-dependent polarization.

We have presented the first systematic study of nuclear tensor polarization measurements made in a laser-driven target. These measurements will be useful as an aid in identifying design changes and technological developments which increase the polarization in the target. For example, better coupling between the glassware and storage cell should improve results and is currently being developed at Argonne. New coating techniques are being examined since wall collisions is the most important relaxation mechanism in the laser-driven target. Both the p_{zz} and P_e measurements provide valuable data for modeling the laser-driven target and, along with the previous work of Walker and Anderson, provide a basis for understanding the nature of the

nuclear and atomic polarization in a laser-driven target. These are the first direct measurements of nuclear polarization in an optical pumped spin-exchange polarized D target and they show that this technology is capable of producing an internal target with nuclear polarization.

Already the results of this work have been used to design the prototype laser driven target installed at IUCF [10]. In this target, the transport tube has been eliminated to avoid the depolarization seen in this work. This will allow higher polarizations even with the constraints of current coating techniques. A major advance with the IUCF prototype target will be the ability to measure the vector polarization p_z as well as p_{zz} using 200 MeV proton scattering. These measurements will be used to fully constrain theoretical models of the polarization distribution in a laser driven target and help determine the optimal operating conditions for a useful target. Because of the large flows available in the laser driven target, even with a modest vector polarization of about 25%, it would provide a better supply of polarized deuterium nuclei than available from an ABS. Since the ultimate goal of this work is to provide a useful polarized target, the IUCF prototype target will provide important results.

Acknowledgements

We thank W. Haeberli, J. van den Brand and the U. of Wisconsin for the loan of many parts of the nuclear polarimeter. We also appreciate the skillful glassblowing of Joe Gregor, who made the glassware depicted in Fig. 3. This work is supported by the U.S. Department of Energy, Nuclear Physics Division, under contract No. W-31-109-ENG-38.

References

[1] K.P. Coulter et al., Phys. Rev. Lett. (1992) 174.
[2] M. Poelker, K.P. Coulter, R.J. Holt, C.E. Jones, R.S. Kowalczyk, L. Young, B. Zeidman, Phys. Rev. A 50 (1994) 2450.
[3] M. Poelker, K.P. Coulter, R.J. Holt, C.E. Jones, R.S. Kowalczyk, L. Young, B. Zeidman, D.K. Toporkov, Nucl. Instr. and Meth. A 364 (1995) 58.
[4] See, e.g., P.L. Anthony et al., Phys. Rev. Lett. 71 (1993) 959.
[5] W. Heil, H. Humblot, E. Otten, M. Schafer, R. Sarkau, M. Leduc, Phys. Lett. A 201 (1995) 337.
[6] K. Zapfe et al., Nucl. Instr. and Meth. A 368 (1996) 293.
[7] DESY Hermes proposal.
[8] MIT-Bates BLAST proposal.
[9] TJNAF experiment number 93-016, C.E. Jones, spokeswoman.
[10] IUCF experiment number CE-68, W.J. Cummings and M. Miller, co-spokesmen.
[11] J.A. Fedchak, C.E. Jones, R.S. Kowalczyk, in: H.P. gen. Schieck, L. Sydow (Eds.), Int. Workshop on Polarized Beams and Polarized Gas Targets, Cologne, 1995, World Scientific, Singapore, 1996, pp. 72–79.
[12] J. Stenger, C. Grosshauser, W. Kilian, B. Ranzenberger, K. Rith, Phys. Rev. Lett. 78 (1997) 4177.
[13] T. Walker, L.W. Anderson, Nucl. Instr. and Meth. A 334 (1993) 313.
[14] W. Happer, Rev. Mod. Phys. 44 (1972) 169.
[15] D. Tupa, L.W. Anderson, D.L. Huber, J.E. Lawler, Phys. Rev. A 33 (1986) 1045.
[16] M.A. Bouchiat, J. Brossel, Phys. Rev. 147 (1966) 41.
[17] J. Stenger, K. Rith, Nucl. Instr. and Meth. A 361 (1995) 60.
[18] T.G. Walker, W. Happer, Rev. Mod. Phys. 69 (1997) 629.
[19] J.A. Fedchak, P. Cabauy, W.J. Cummings, C.E. Jones, R.S. Kowalczyk, Nucl. Instr. and Meth. A 391 (1997) 405.
[20] J.S. Price, W. Haeberli, Nucl. Instr. and Meth. A 326 (1993) 416.
[21] G.G. Ohlsen, J.L. McKibben, G.P. Lawrence in: H.H. Barschall, W. Haeberli (Eds.), Polarization Phenomena in Nuclear Reactions, Proc. 3rd Int. Symp., Madison, 1970, The University of Wisconsin Press, Madison, 1971, pp. 503–505.